

Black hole evolution: II. Spinning black holes in a supernova-driven turbulent interstellar medium

Yohan Dubois^{1,2*}, Marta Volonteri^{1,3}, Joseph Silk^{1,2,4}, Julien Devriendt^{2,5} and Adrienne Slyz²

¹ *Institut d’Astrophysique de Paris, UMR 7095, CNRS, UPMC Univ. Paris VI, 98 bis boulevard Arago, 75014 Paris, France*

² *Sub-department of Astrophysics, University of Oxford, Keble Road, Oxford OX1 3RH*

³ *Astronomy Department, University of Michigan, Ann Arbor, MI 48109, USA*

⁴ *Department of Physics and Astronomy, The Johns Hopkins University Homewood Campus, Baltimore, MD 21218, USA*

⁵ *Observatoire de Lyon, UMR 5574, 9 avenue Charles André, Saint Genis Laval 69561, France*

Accepted . Received ; in original form

ABSTRACT

Supermassive black holes (BH) accrete gas from their surroundings and coalesce with companions during galaxy mergers, and both processes change the BH mass and spin. By means of high-resolution hydrodynamical simulations of galaxies, either idealised or embedded within the cosmic web, we explore the effects of interstellar gas dynamics and external perturbations on BH spin evolution. All these physical quantities were evolved on-the-fly in a self-consistent manner. We use a ‘maximal’ model to describe the turbulence induced by stellar feedback to highlight its impact on the angular momentum of the gas accreted by the BH. Periods of intense star formation are followed by phases where stellar feedback drives large-scale outflows and hot bubbles. We find that BH accretion is synchronised with star formation, as only when gas is cold and dense do both processes take place. During such periods, gas motion is dominated by consistent rotation. On the other hand, when stellar feedback becomes substantial, turbulent motion randomises gas angular momentum. However BH accretion is strongly suppressed in that case, as cold and dense gas is lacking. In our cosmological simulation, at very early times ($z > 6$), the galactic disc has not yet settled and no preferred direction exists for the angular momentum of the accreted gas, so the BH spin remains low. As the gas settles into a disc ($6 > z > 3$), the BH spin then rapidly reaches its maximal value. At lower redshifts ($z < 3$), even when galaxy mergers flip the direction of the angular momentum of the accreted gas, causing it to counter-rotate, the BH spin magnitude only decreases modestly and temporarily. Should this be a typical evolution scenario for BH, it potentially has dramatic consequences regarding their origin and assembly, as accretion on maximally spinning BH embedded in thin Shakura-Sunyaev disc is significantly reduced.

Key words: galaxies: ISM — galaxies: active — quasars: supermassive black holes — galaxies: high-redshift — methods: numerical

1 INTRODUCTION

Supermassive black holes (BH) are compact objects commonly observed in the centre of galaxies. They are suspected to grow along with their host galaxies as observations suggest a strong scaling between BH masses and galaxy properties (Magorrian et al. 1998; Tremaine et al. 2002; Häring & Rix 2004). Gas accretion, as opposed to

mergers, drives most of the mass growth of black holes at high-redshift (Yu & Tremaine 2002; Dubois et al. 2013; Kulier et al. 2013) either through direct accretion of cosmic filamentary gas or of star-forming clumps (Bournaud et al. 2011; Di Matteo et al. 2012; Dubois et al. 2012, 2013; Bellovary et al. 2013; Feng et al. 2013). This mechanism converts a fraction of the accreted rest-mass energy into effective feedback for the host galaxy, which in turn can explain the observed scaling relation between black holes and galaxies (Silk & Rees 1998; King 2003; Wyithe & Loeb

* E-mail: dubois@iap.fr

2003). Such a behaviour has been successfully implemented in modern cosmological simulations, and the impact of active galactic nucleus (AGN) feedback on galaxy properties can be dramatic (Di Matteo et al. 2005; Croton et al. 2006; Bower et al. 2006; Sijacki et al. 2007; Booth & Schaye 2009; Dubois et al. 2010; Teyssier et al. 2011; Dubois et al. 2012).

In thin accretion discs (e.g., Shakura & Sunyaev 1973), the radiative efficiency, i.e., the fraction of energy released and radiated during accretion events on to central BHs can be related directly to the spin magnitude, via the potential energy, E_{ischo} , of a particle on the innermost stable orbit: $\epsilon_r = 1 - E_{\text{ischo}} = 1 - \sqrt{1 - 2/(3r_{\text{ischo}})}$. Since the last stable orbit, r_{ischo} , is closer in for BHs with high spin, corotating with the accretion disc, they liberate more energy than non-spinning or counter-rotating BHs at fixed accretion rate. Therefore, the magnitude and relative orientation of BH spins has a direct consequence on the mass growth, as the maximum rate at which BHs accrete, the Eddington limit, is inversely proportional to radiative efficiency of the accretion process: highly spinning BHs grow more slowly than BHs with lower spin values. Consequently, the rate at which the high-redshift BHs are able to gain their mass as observed above $z > 6$ (Fan & et al., 2006; Jiang & et al., 2009; Mortlock & et al., 2011; Johnson et al. 2013) underscores the need to jointly study BH mass and spin evolution.

The current measurements of spins through X-ray spectroscopy still have large uncertainties or controversial measurements (see the recent review by Reynolds 2013, and references therein) due to degeneracies in the underlying models that try to reproduce the observed spectral energy distribution of AGN. Therefore, theoretical models and numerical simulations could provide powerful tools for predicting spin values and interpreting the data more precisely. Theoretical models (Moderski & Sikora 1996a,b; Moderski et al. 1998) forecast that BH spin grows to large values if the angular momentum (AM) of the accreted material onto the BH is aligned with that of the BH or has some level of coherency. A completely random distribution of the accreted gas AM is needed to drive BH spins towards zero (King et al. 2008; Dotti et al. 2013). In this paper, we take advantage of isolated galaxy simulations and a direct cosmological simulation performed at high spatial and mass resolution to study the effect of turbulence in the ISM on the distribution of gas AM. More specifically, we investigate whether the motion of interstellar gas reaches a chaotic state such that the gas AM reorients on a short time-scale (shorter than a Salpeter time-scale).

Some recent numerical work have been undertaken by different authors that led to divergent results: Maio et al. (2013) use GADGET (Springel 2005) to run simulations at very high spatial resolution, and follow star formation and supernova (SN) feedback (but not BH feedback) self-consistently down to sub-pc scale, but adopt an idealised set-up, i.e. a massive circumnuclear disc within an external bulge potential. They find that, independently of resolution and feedback prescriptions, the gas that feeds the BH has a net AM aligned with that of the circumnuclear disc, despite the high level of turbulence induced by motions of gas clumps and stellar feedback. Conversely, Hopkins et al. (2012) use a series of nested simulations run with GADGET to track the AM of gas flowing from kpc to pc scales. They start from representative examples of gas-rich mergers

and isolated, moderately bar-unstable disc simulations, and through a series of resimulations, reach a resolution limit of 0.1 pc. While they do not explicitly model stellar or BH feedback but use an effective equation of state instead, the advantage of their strategy is that the large-scale torques due to galaxy mergers and bar instabilities are taken into account. In these simulations, they often find misalignments between the inner 1 pc gas AM and that at large scales (even though they do not follow the spin evolution of a central BH) resulting from a galaxy merger.

This paper is part of a series of three papers investigating the connection between SN feedback and BH growth (Dubois et al. 2013, paper I), SN-driven gas turbulence and BH spin evolution, (this paper, paper II), and the impact of galaxy evolution on the spin of a cosmologically representative sample of central BH (Dubois et al. 2013, paper III). The main purpose here is to investigate the spin (and mass) evolution of a central BH in high-resolution hydrodynamical simulations, including a cosmological run. This allows one to assess, albeit in a specific case, the influence of galaxy mergers and simultaneously probe how gas on galaxy scales connects to the inner region surrounding the BH. The simulations have enough resolution, 10 pc, to start resolving the substructures of the ISM over several rotation periods of the galactic disc ($\sim 50 - 100$ Myr in our simulations). Moreover, we use the recent non-thermal SN feedback prescription from Teyssier et al. (2013) to maximize the level of gas turbulence present in the galaxy. The idea behind such a numerical set-up is to provide as low a level of coherence in the AM flowing to the BH as possible.

In Section 2 we introduce the initial conditions and the numerical models for the physics of galaxy formation, BH mass growth and its associated AGN feedback. In Section 3 we provide a detailed description as to how BH spin evolves in our simulations, which depends on gas accretion and BH-BH mergers. In Section 4 we detail our results for the evolution of BH spin in an isolated galaxy and for a BH with similar mass embedded within its cosmological environment. Finally, in Section 5 we discuss our results.

2 NUMERICAL SET-UP

The simulations are run with the Adaptive Mesh Refinement code RAMSES (Teyssier 2002). The evolution of the gas is followed using a second-order unsplit Godunov scheme for the Euler equations. The HLLC Riemann solver with a first-order MinMod Total Variation Diminishing scheme to reconstruct the interpolated variables from their cell-centered values is used to compute fluxes at cell interfaces. Collisionless particles (DM, star and BH particles) are evolved using a particle-mesh solver with a Cloud-In-Cell interpolation.

2.1 Isolated galaxy

For the isolated galaxy run, the gas is initially set in hydrostatic equilibrium within a live NFW (Navarro et al. 1997) dark matter (DM) halo with a concentration parameter $c = 3.5$. The total mass of gas plus DM is $M_{\text{vir}} = 10^{12} M_{\odot}$. The gas fraction is 15 per cent, and the gas has some initial AM with a total spin parameter of 0.04, slightly lower but consistent with the average spin parameter of cosmological

dark matter halos (Bullock et al. 2001). When the simulation starts, the gas loses its internal pressure support due to gas cooling and a centrifugally supported disc settles in the centre of the gravitational potential well.

The mass of a DM particle is $M_{\text{DM,res}} = 1.7 \times 10^6 M_{\odot}$, and the minimum grid cell size is of $\Delta x = 9$ pc. A central BH is inserted after 60 Myr, when the gas density has become sufficiently high to start forming stars, with an initial seed mass of $10^4 M_{\odot}$. A resolution study is presented in Appendix A.

2.2 Cosmological galaxy

We assume a Λ CDM cosmology with total matter density $\Omega_m = 0.3$, baryon density $\Omega_b = 0.045$, dark energy density $\Omega_{\Lambda} = 0.7$, amplitude of the matter power spectrum $\sigma_8 = 0.8285$, $n_s = 0.9635$ spectral index and Hubble constant $H_0 = 68.14 \text{ km s}^{-1} \text{ Mpc}^{-1}$ consistent with the Planck data (Planck Collaboration et al. 2013) for the initial conditions produced with MUSIC (Hahn & Abel 2011). The box size of our simulation is $L_{\text{box}} = 50 h^{-1} \text{ Mpc}$, with a coarse grid of 256^3 DM particles corresponding to a DM mass resolution of $M_{\text{res,coarse}} = 8 \times 10^8 M_{\odot}$. A high-resolution region is defined around a halo of $M_{\text{vir}} = 10^{12} M_{\odot}$ at $z = 2$ that contains only high-resolution DM particles within $2 r_{\text{vir}}$ ($r_{\text{vir}} = 100$ kpc) with mass $M_{\text{res,high}} = 2 \times 10^5 M_{\odot}$.

The mesh is refined up to $\Delta x = 8.7$ pc (maximum level of refinement equals 21 at redshift $z = 3$) using a quasi-Lagrangian strategy: we refine when the mass in a cell becomes larger than 8 times the mass of our high resolution DM particles. The minimum cell size is kept roughly constant in physical size with redshift, i.e. an additional level of refinement is added every $a_{\text{exp}} = n \times 0.1$ (where $n = 1, 2, 4, 8$ and a_{exp} is the expansion factor of the universe) up to level 21 at $a_{\text{exp}} = 0.33$. The BH seed mass used in the cosmological simulation is larger than for the isolated runs, at $10^5 M_{\odot}$.

Such a high spatial resolution for a cosmological zoomed halo evolved over several billion years places this simulation amongst the most resolved state-of-the hydrodynamical cosmological simulation including complex sub-grid processes to date. We call this simulation and its various flavours (resolution, physics) the SETH simulation suite¹.

2.3 Physics of galaxy formation

Gas is allowed to cool by H and He cooling with a contribution from metals using a Sutherland & Dopita (1993) model for temperatures above $T_0 = 10^3$ K, which is the minimum temperature we allow the gas to reach through radiative losses. Heating from a uniform UV background takes place after redshift $z_{\text{reion}} = 10$ following Haardt & Madau (1996). Metallicity is modelled as a passive variable for the gas advected with the flow (whose composition is assumed to be solar) and is altered by gas ejecta from SN explosions and stellar winds. We assume a zero initial metallicity. The gas

follows the equation of state (EoS) of an ideal monoatomic gas with adiabatic index $\gamma = 5/3$.

The star formation process is modelled with a Schmidt law: $\dot{\rho}_* = \epsilon_* \rho / t_{\text{ff}}$, where $\dot{\rho}_*$ is the star formation rate density, ϵ_* the constant star formation efficiency, and t_{ff} the local free-fall time of the gas. We choose a low star formation efficiency $\epsilon_* = 0.02$ consistent with observations of giant molecular clouds (Krumholz & Tan 2007) and surface density relations of galaxies (Kennicutt 1998). Star formation is allowed in regions exceeding a gas density threshold of $n_0 = 250 \text{ H cm}^{-3}$ and for gas with a temperature given by the polytropic EoS described below. The minimum mass of a star particle is $m_{\text{s,res}} = n_0 \Delta x^3 \simeq 4 \times 10^3 M_{\odot}$ at our spatial resolution $\Delta x = 9$ pc. The gas pressure is artificially enhanced above $\rho > \rho_0$ assuming a polytropic EoS $T = T_0 (\rho / \rho_0)^{\kappa-1}$ with polytropic index $\kappa = 2$ to avoid spurious gas fragmentation: we always resolve the Jeans length with at least four cells. Feedback from massive stars is taken into account assuming a Salpeter initial mass function with $\eta_{\text{SN}} = 0.1$ of the mass fraction of stars ending up as type II SN and releasing $10^{50} \text{ erg } M_{\odot}^{-1}$. We use the feedback model introduced in (Teyssier et al. 2013, similar in spirit to the delayed cooling prescription from Stinson et al. 2006), where energy is released both as a thermal component and a tracer, “non-thermal” component, which is passively advected with the flow. This passive non-thermal energy decays on a typical time-scale of $t_{\text{diss}} = 0.8$ Myr, and gas cooling is prevented until the velocity dispersion associated with this non-thermal energy component becomes larger than $\sigma_{\text{NT}} = 50 \text{ km.s}^{-1}$. In isolated dwarf galaxies, this allows for an efficient driving of large-scale galactic winds and turbulence in the interstellar medium (ISM) as shown in Teyssier et al. (2013).

An alternative modelling of SNe feedback through kinetic Sedov blast wave explosions (Dubois & Teyssier 2008) and its impact on the BH spin evolution is presented in the Appendix B. Its relative impact on the BH growth compared to the reference case is the topic of Paper I.

2.4 Model for BH growth and AGN feedback

We use the same “canonical” BH model employed in Dubois et al. (2012). BH are created at loci where gas density is larger than the density threshold for star formation ρ_0 with an initial seed mass of 10^4 or $10^5 M_{\odot}$ (respectively for the isolated and the cosmological simulations). In order to avoid the formation of multiple BH in the same galaxy, BH are not allowed to form at distances smaller than 50 kpc from any other BH particle. The accretion rate onto BH follows the Bondi-Hoyle-Lyttleton (Bondi 1952) rate $\dot{M}_{\text{BH}} = 4\pi\alpha G^2 M_{\text{BH}}^2 \bar{\rho} / (\bar{c}_s^2 + \bar{u}^2)^{3/2}$, where M_{BH} is the BH mass, $\bar{\rho}$ is the average gas density, \bar{c}_s is the average sound speed, \bar{u} is the average gas velocity relative to the BH velocity, and α is a dimensionless boost factor with $\alpha = (\rho / \rho_0)^2$ when $\rho > \rho_0$ and $\alpha = 1$ otherwise (Booth & Schaye 2009) in order to account for our inability to capture the colder and higher density regions of the ISM which are suppressed by the presence of the polytropic EoS. The effective accretion rate onto BH is capped at the Eddington accretion rate: $\dot{M}_{\text{Edd}} = 4\pi G M_{\text{BH}} m_p / (\epsilon_r \sigma_T c)$, where σ_T is the Thompson cross-section, c is the speed of light, m_p is the proton mass, and ϵ_r is the radiative effi-

¹ The name is a reference to the Egyptian god of desert, storms, disorder and violence. It is also a reference to the code employed for the simulations, RAMSES, and suite of simulations with similar (as well as much higher) resolution performed for a lower mass galaxy at high redshift, the NUT suite (Powell et al. 2011).

ciency, assumed to be proportional to the spin of the BH with $\epsilon_r = 1 - E_{\text{isco}} = 1 - \sqrt{1 - 2/(3r_{\text{isco}})}$.

In order to avoid spurious oscillations of the BH in the gravitational potential well due to external perturbations and finite resolution effects, we introduce a drag force that mimics the dynamical friction exerted by the gas onto a massive particle. This dynamical friction is proportional to $F_{\text{DF}} = f_{\text{gas}} 4\pi\alpha\rho(GM_{\text{BH}}/\bar{c}_s)^2$, where f_{gas} is a fudge factor whose value is between 0 and 2 and is a function of the mach number $\mathcal{M} = \bar{u}/\bar{c}_s < 1$ (Ostriker 1999; Chapon et al. 2013), and where we introduce the boost factor α for reasons previously stated.

Two BH are allowed to merge when the distance separating the two particles is smaller than $4 \times \Delta x$ and when their relative velocity is smaller than the escape velocity of the binary.

The AGN feedback is a combination of two different modes, the so-called *radio* mode operating when $\chi = \dot{M}_{\text{BH}}/\dot{M}_{\text{Edd}} < 0.01$ and the *quasar* mode active otherwise. The quasar mode corresponds to an isotropic injection of thermal energy into the gas within a sphere of radius Δx , with an energy deposition rate: $\dot{E}_{\text{AGN}} = \epsilon_f \epsilon_r \dot{M}_{\text{BH}} c^2$, where $\epsilon_f = 0.15$ is a free parameter chosen to reproduce the $M_{\text{BH}}-M_b$, $M_{\text{BH}}-\sigma_b$, and BH density in our local Universe (see Dubois et al. 2012). At low accretion rates, on the other hand, the radio mode deposits the AGN feedback energy into a bipolar outflow with a jet velocity of 10^4 km.s^{-1} into a cylinder with a cross-section of radius Δx and height $2\Delta x$ following Omma et al. (2004) (more details about the jet implementation are given in Dubois et al. 2010). The efficiency of the radio mode is larger with $\epsilon_f = 1$.

3 MODEL OF BH SPIN EVOLUTION

3.1 Gas accretion

BH spins are allowed to change by accretion of gas through the following expression (Bardeen 1970):

$$a^{n+1} = \frac{1}{3} \frac{r_{\text{isco}}^{1/2}}{M_{\text{ratio}}^n} \left[1 - \left(3 \frac{r_{\text{isco}}}{M_{\text{ratio}}^2} - 2 \right)^{1/2} \right], \quad (1)$$

where $M_{\text{ratio}} = M_{\text{BH}}^{n+1}/M_{\text{BH}}^n$, the n superscript stands for the values at time t_n , and R_{isco} is the radius of the innermost stable circular orbit (ISCO) defined as (in reduced units):

$$r_{\text{isco}} = R_{\text{isco}}/R_g = 3 + Z_2 \pm [(3 - Z_1)(3 + Z_1 + 2Z_2)]^{1/2}, \quad (2)$$

where the gravitational radius R_g is defined as half of the Schwarzschild radius of the BH, R_{BH} , and Z_1 and Z_2 are:

$$Z_1 = 1 + (1 - a^2)^{1/3} [(1 + a)^{1/3} + (1 - a)^{1/3}], \quad (3)$$

$$Z_2 = (3a^2 + Z_1^2)^{1/2}. \quad (4)$$

For spins co-rotating with their accretion disc, $1 \leq r_{\text{isco}} < 6$, while for spins counter-rotating with their accretion disc, $6 < r_{\text{isco}} \leq 9$, and $r_{\text{isco}} = 6$ for non-spinning BH.

Equation 1, governing the evolution of the BH spin magnitude through direct accretion of gas, assumes that BH spin and disc AM are perfectly aligned (or anti-aligned), but in the most general case, misalignments occur. In the misaligned case, the accretion disc experiences a torque due to the Lense-Thirring effect that causes the accretion disc

to precess about the spin axis of the BH. For large enough viscosities the innermost parts of the disc are forced to rotate within the equatorial plane of the disc and a warped disc is created. We can define the total AM of the system {disc+BH} as $\mathbf{J}_{\text{tot}} = \mathbf{J}_{\text{d}} + \mathbf{J}_{\text{BH}}$. The values of the angle θ between \mathbf{J}_{BH} and \mathbf{J}_{d} are between $-1 \leq \cos \theta \leq 1$ where the two extrema correspond to anti-aligned and aligned cases respectively.

The result of the Lense-Thirring precession is that the BH and disc AM end up being aligned or anti-aligned with the total AM. The case for anti-alignment of the BH with the disc requires that (King et al. 2005)

$$\cos \theta < -\frac{J_{\text{d}}}{2J_{\text{BH}}}, \quad (5)$$

thus, for $\cos \theta \geq 0$, they always align, while for $\cos \theta < 0$, they eventually anti-align if the ratio $J_{\text{d}}/J_{\text{BH}}$ is sufficiently small compared to $\cos \theta$.

One difficulty we experience is in accessing the magnitude of \mathbf{J}_{d} as we cannot resolve the accretion disc in our simulations. We therefore assume the tilted solution for a thin accretion disc (Shakura & Sunyaev 1973; Scheuer & Feiler 1996a; Natarajan & Pringle 1998; Pereo et al. 2009), characterized by a viscosity $\nu_1 = \alpha_t \bar{c}_s^2 / (GM_{\text{BH}}/r^3)^{1/2}$, where α_t is a parameter < 1 , and c_s is the sound speed. In a misaligned disc under the effect of Lense-Thirring precession a natural scale is the warp radius, that marks the transition between an equatorial inner disc and a misaligned outer disc: the direction of the AM of the inflowing material changes direction as it passes through the warp. Only material within the warp radius can effectively transfer its AM to the BH (Volonteri et al. 2007). This is the relevant scale to estimate whether alignment or anti-alignment occur. In a Shakura & Sunyaev (1973) thin accretion disc, one can write the ratio of the warp to Schwarzschild radius as:

$$\frac{R_{\text{warp}}}{R_{\text{BH}}} \simeq 6.4 \times 10^3 a^{5/8} M_{\text{BH},8}^{1/8} \left(\frac{\epsilon_{r,01}}{\chi} \right)^{1/4} \left(\frac{\nu_2}{\nu_1} \right)^{-5/8} \alpha_{t,01}^{-1/2}, \quad (6)$$

where $\epsilon_{r,01}$ is the radiative efficiency normalised to 0.1, ν_1 and ν_2 are the kinematic viscosities horizontal and perpendicular to the equatorial plane of the disc: ν_2 is the viscosity responsible the warp propagation, while ν_1 is the viscosity responsible for driving accretion and transferring AM. We choose a value for $\alpha_{t,01} \equiv \alpha_t/0.1 = 1$ (King et al. 2007), and the ratio of $\nu_2/\nu_1 = 2(1 + 7\alpha_t)/(4 + \alpha_t^2)/\alpha_t^2$ is of the form given by Ogilvie (1999) (equation 145). With these choices, $(\nu_2/\nu_1) \sim 85$ (note that for small α_t , $\nu_2 \sim \nu_1/\alpha_t^2$) and:

$$\frac{R_{\text{warp}}}{R_{\text{BH}}} \simeq 4 \times 10^2 a^{5/8} M_{\text{BH},8}^{1/8} \left(\frac{\epsilon_{r,01}}{\chi} \right)^{1/4} \left(\frac{\nu_2/\nu_1}{85} \right)^{-5/8} \alpha_{t,01}^{-1/2}. \quad (7)$$

The BH AM is simply $J_{\text{BH}} = aM_{\text{BH}}^{3/2} R_{\text{BH}}^{1/2}$, and the disc AM can now be expressed as $J_{\text{d}} \sim M_{\text{d}}(R_{\text{warp}}) M_{\text{BH}}^{1/2} R_{\text{warp}}^{1/2}$. The disc mass within R_{warp} is $M_{\text{d}}(R_{\text{warp}}) = M t_{\nu_1}(R_{\text{warp}})$ where t_{ν_1} is the viscous timescale for radial propagation:

$$t_{\nu_1} = 5.3 \times 10^5 a^{7/8} M_{\text{BH},8}^{11/8} \left(\frac{\epsilon_{r,01}}{\chi} \right)^{3/4} \left(\frac{\nu_2}{\nu_1} \right)^{-7/8} \alpha_t^{-3/2} \text{yr} \quad (8)$$

$$\sim 3.4 \times 10^5 a^{7/8} M_{\text{BH},8}^{11/8} \left(\frac{\epsilon_{r,01}}{\chi} \right)^{3/4} \left(\frac{\nu_2/\nu_1}{85} \right)^{-7/8} \alpha_{t,01}^{-3/2} \text{yr}.$$

The ratio of disc to BH AM can then be written as:

$$\frac{J_d}{2J_{\text{BH}}} \simeq \frac{M_d(R_{\text{warp}})}{aM_{\text{BH}}} \left(\frac{R_{\text{warp}}}{R_{\text{BH}}} \right)^{1/2} \quad (9)$$

$$\sim 6.8 \times 10^{-2} \left(\frac{\chi}{\epsilon_{r,01}} \right)^{1/8} M_{\text{BH},8}^{23/16} a^{3/16} \alpha_{t,01}^{-7/4} \left(\frac{\nu_2/\nu_1}{85} \right)^{-19/16}.$$

Equation (9) allows one to evaluate if anti-alignment occurs, and provides a value for the magnitude of J_d . We refer the reader to Dotti et al. (2013) for a detailed discussion of how the ratio J_d/J_{BH} determines the behaviour of alignment and spin evolution.

For the direction of J_d , we assume that the accretion disc is aligned with the gas AM, J_g , measured in the surroundings of the BHs as extracted directly in the simulation (on $\Delta x = 10$ pc scale). We update the orientation of the BH AM after one accretion event of $\Delta t = t_{\nu_1}$ with $J_{\text{BH}}^{n+1} = J_{\text{tot}} = J_{\text{BH}}^n + J_d^n j_g^n$ for the alignment case, where the small j stands for AM unit vectors, and where J_d^n is provided by equation (9). If the criterion for anti-alignment is met, J_{BH}^{n+1} becomes $-J_{\text{tot}}$ if $J_{\text{tot}} \cdot J_{\text{BH}}^n > 0$, this occurs when the total AM dominated by the BH (case b in Fig. 1 of King et al. 2005). Otherwise, if the anti-alignment condition is satisfied and $J_{\text{tot}} \cdot J_{\text{BH}}^n < 0$, then the total AM is dominated by the disc and it is anti-aligned with respect to that of the BH, therefore $J_{\text{BH}}^{n+1} = J_{\text{tot}}$ (case d in Fig. 1 of King et al. 2005).

For sufficiently large accretion rates, accretion discs can become unstable against their own gravity and fragment into gas clumps (e.g. Kolykhalov & Syunyaev 1980; Pringle 1981; Goodman & Tan 2004). The criterion for stability given by the Toomre parameter $Q \sim c_s \Omega / (\pi G \Sigma)$, where Ω is the Keplerian velocity and Σ the gas surface density, provides the radius R_{sg} below which the accretion disc is stable. For the standard α -disc external region:

$$\frac{R_{\text{sg}}}{R_{\text{BH}}} \simeq 5 \times 10^2 \alpha_{t,01}^{28/45} M_{\text{BH},8}^{-52/45} \left(\frac{\epsilon_{r,01}}{\chi} \right)^{22/45}, \quad (10)$$

and the mass stable against fragmentation is (see Dotti et al. 2013)

$$M_{\text{sg}} \simeq 6 \times 10^5 \alpha_{t,01}^{-1/45} M_{\text{BH},8}^{34/45} \left(\frac{\chi}{\epsilon_{r,01}} \right)^{4/45} M_{\odot}. \quad (11)$$

We include the effects of self-gravity when $R_{\text{sg}} < R_{\text{warp}}$. In this case, the outer region of the disc is subject to fragmentation, while the central region as a whole aligns (or anti-aligns) in the equatorial plane of the BH. Then, the AM accreted onto the BH is the form of equation (9) with R_{warp} and $M_d(R_{\text{warp}})$ replaced by R_{sg} and M_{sg} respectively. Thus, we repeat the same steps as for the non self-gravitating case for the alignment (anti-alignment) criterion with the AM calculated with R_{sg} and M_{sg} . In contrast to King et al. (2008), who assume that self-gravity causes chaos in the AM distribution, we argue that the accreted gas conserves the AM direction it possessed when entering the accretion flow, which is the direction measured from the simulation by definition. As a final note, the effects of self-gravity become important when $R_{\text{sg}} < R_{\text{warp}}$, and through Eq. (7) and (10), the critical BH mass above which the BH cannot stabilise anymore the disc against fragmentation is:

$$M_{\text{BH},8} > 1.15 a^{-\frac{225}{461}} \left(\frac{\epsilon_{r,01}}{\chi} \right)^{\frac{86}{461}} \left(\frac{\nu_2/\nu_1}{85} \right)^{\frac{225}{461}} \alpha_{t,01}^{\frac{404}{461}}. \quad (12)$$

Similar expressions hold when using the middle region solutions for the α -disc. In this case $R_{\text{sg}}/R_{\text{BH}} \simeq 10^3 \alpha_{t,01}^{14/27} M_{\text{BH},8}^{-26/27} (\epsilon_{r,01}/\chi)^{8/27}$ and the radius where self-gravity truncates the disc becomes smaller than the warp radius when $M_{\text{BH},8} > 2.23 a^{-\frac{135}{269}} (\epsilon_{r,01}/\chi)^{\frac{10}{269}} [(\nu_2/\nu_1)/85]^{\frac{135}{269}} \alpha_{t,01}^{\frac{220}{269}}$.

Our implementation is based on analytical studies, as we cannot self-consistently include an accretion disc (on milli-pc scales) in a galaxy formation simulation. Regarding numerical studies of BH spin-disc alignment we recall that Fragile & Anninos (2005), Fragile et al. (2007), and Dexter & Fragile (2011) find no alignment in their three-dimensional general relativistic magnetohydrodynamic simulations of relatively thick, low-accretion rate tilted discs, where however alignment is not expected to occur, as the typical accretion rate is sufficiently low that alignment would not occur in a Hubble time (Dexter & Fragile 2011). Recently Sorathia et al. (2013) study the alignment process in magnetohydrodynamic simulations of relatively thin disks and find instead that the BH and the disc progressively align, inside-out. While, at the time being, it is not trivial to derive an analytical description of their simulations accurate enough to be explicitly included in our simulations, we use an extrapolation of their order-of-magnitude estimates to obtain, in turn, a qualitative validation of our methodology. We consider their suggestion that the inclination transition radius (roughly analogue to what we call warp radius here) can be expressed as $R_T \sim 0.5 \Phi a^{2/3} (H/R_T)^{-4/3} R_{\text{BH}}$, where $1 < \Phi < \alpha^{-2/3}$ and (H/R_T) is the disc aspect ratio. We also assume that the alignment timescale is of order the alignment propagation radius at R_T (Eq. 13 in Sorathia et al. 2013). Assuming the middle region solutions for the α -disc we find an upper limit to the alignment timescale of $\sim 10^5 a^{7/8} M_8^{11/8} \alpha^{-15/4} \left(\frac{\chi}{\epsilon_{r,01}} \right)^{-3/4} \Phi^{45/16}$ yr by minimising the propagation rate of the alignment front. While this alignment timescale is very similar to our previous estimates and with the implementation in RAMSES, since the estimate we obtain is approximate, we discuss in Appendix C how our results would be modified if the alignment timescale is much longer than these estimates suggest.

3.2 Coalescence of BHs

We track the change of the spin during the coalescence of two BH using the analytical fit of Rezzolla et al. (2008) derived from relativistic numerical simulations of BH binaries. The final value of spin of the BH remnant is

$$\mathbf{a} = \frac{1}{(1+q)^2} (\mathbf{a}_1 + \mathbf{a}_2 q^2 + \ell q), \quad (13)$$

where \mathbf{a}_1 is the spin vector of the most massive BH progenitor, \mathbf{a}_2 is the spin vector of the least massive BH progenitor, $q = M_2/M_1 \leq 1$ the mass ratio of the binary, and $\ell = \mathbf{l}/(M_1 M_2)$, with \mathbf{l} the difference between the orbital AM \mathbf{L} when the two BHs are widely separated and the AM \mathbf{J}_{gw} extracted from gravitational waves before the final coalescence $\mathbf{l} = \mathbf{L} - \mathbf{J}_{\text{gw}}$.

Rezzolla et al. (2008) provides a simple analytical expression for the norm of ℓ

$$\begin{aligned} \ell = & \frac{s_4}{(1+q^2)^2} (a_1^2 + a_2^2 q^4 + 2\mathbf{a}_1 \cdot \mathbf{a}_2 q^2) \\ & + \frac{s_5 \mu + t_0 + 2}{1+q^2} (a_1 \cos \phi_1 + a_2 q^2 \cos \phi_2) \\ & + 2\sqrt{3} + t_2 \mu + t_3 \mu^2, \end{aligned} \quad (14)$$

where ϕ_1 (ϕ_2) is the angle between \mathbf{a}_1 (\mathbf{a}_2) and ℓ , and $\mu = q/(1+q)^2$. We made the same assumption than Rezzolla et al. (2008) to get the direction of ℓ by imposing collinearity with the orbital AM $\mathbf{L} = \mathbf{L}_1 + \mathbf{L}_2$ before coalescence, which is a vector directly measured in our simulations. To get access to \mathbf{L} , we compute the centre of mass of the binary \mathbf{r}_{com} and we evaluate the AM of the two BHs relative to the centre of mass with $\mathbf{L}_1 = M_1(\mathbf{r}_1 - \mathbf{r}_{\text{com}}) \times (\mathbf{v}_1 - \mathbf{v}_{\text{com}})$. The numerical constants involved in equation (14) are equal to $s_4 = -0.129$, $s_5 = -0.384$, $t_0 = -2.686$, $t_2 = -3.454$, and $t_3 = 2.353$.

Finally we neglect the mass loss during BH-BH coalescence through gravitational waves, which is typically of the order of 5 per cent (Rezzolla et al. 2008), and we also neglect the recoil kick velocity received by the BH remnant that can be up to several 1000 km s^{-1} (e.g. Baker et al. 2007; Campanelli et al. 2007a,b) for the most extreme cases and lead to a population of wandering BHs (Libeskind et al. 2006; Volonteri & Madau 2008; Volonteri et al. 2010; Sijacki et al. 2011), an effect probably tempered by gas dynamical friction acting on kicked BHs (Sijacki et al. 2011).

3.3 Updating spins

We assume that the initial spin of BHs is zero at creation. We further assume that the thin disc solution for spin evolution applies at any accretion rate over Eddington χ . It seems to be a fairly good approximation as BH spins mostly change their value by accretion during strong accretion events (of the order of $\chi \lesssim 1$). The maximum spin value that we authorise is $a_{\text{max}} = 0.998$, due to the capture by the central BH of radiated photons emitted from the accretion disc (Thorne 1974). In the case of thick discs, however, we note that (Gammie et al. 2004) find in their numerical simulations that $a_{\text{max}} \sim 0.9 - 0.93$, taking into account the magneto-hydrodynamical effects on the transfer of gas AM, while Sądowski et al. (2011) suggest that super-critical accretion discs allow a maximal spin up to $a_{\text{max}} = 0.9994$ in low-viscosity, $\alpha_t = 0.01$, accretion discs.

As we treat the spin evolution on-the-fly, radiative efficiencies, and, thus, Eddington accretion rate and bolometric luminosities vary with the amplitude of the BH spin. Also, the jet of the radio mode of AGN feedback is launched along the spin axis of the BH.

4 RESULTS

4.1 The isolated galaxy

4.1.1 Evaporation of the dense star-forming gas

Fig. 1 shows the star formation rate (SFR) of the isolated galaxy over 1 Gyr of evolution. The SFR is bursty with peaks

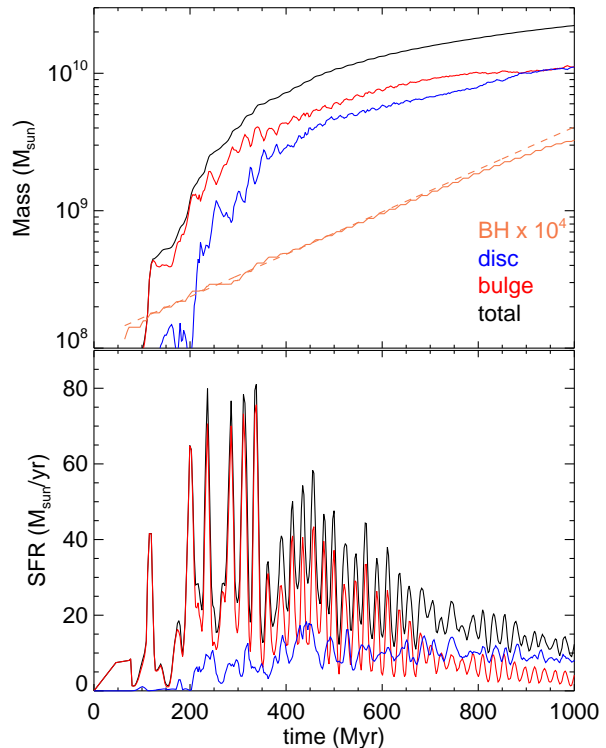


Figure 1. Isolated galaxy simulation. *Top panel:* Total stellar mass (black), stellar mass within $r \leq 500$ pc around the centre of the simulation box (red), disc (total minus bulge in blue), and 10^4 times the BH mass ($\times 10^4$) growing at half the Eddington rate of a maximum spinning BH ($\epsilon_r = 0.32$) is represented by the orange dashed line. *Bottom panel:* Star formation rate as a function of time for the entire galaxy (black), for the stars within the bulge $r \leq 500$ pc (red), and within the disc (blue). The SFR in the bulge shows large variations due to the regular outflows produced by SN explosions, while the SFR is more steady in the disc. The BH grows in synchronisation with the peaks of the bulge SFR.

of SFR larger than $50 M_{\odot} \text{ yr}^{-1}$, and with an average value around $20 - 30 M_{\odot} \text{ yr}^{-1}$. The large oscillations observed are due to the self-regulation of the cold star-forming gas in the ISM by SNe explosions (Teyssier et al. 2013). Here the peaks of the SFR are dominated by the activity within the bulge², $r \leq 500$ pc, of the galaxy, while the average level of the SFR corresponds to the SFR in the disc of the galaxy within cold dense clumps. During the beginning of the collapse of the halo $t \leq 400$ Myr, several galactic outflows develop up to $5 - 10$ kpc distance above the plane of the disc (see top panel of Fig. 2). However, due to the strong pressure confinement exerted by the ram-pressure of the hot infalling gas, the outflowing gas is maintained within that region and falls back onto the galaxy in a cycle of galactic fountain (Dubois & Teyssier 2008). Later on, after $t > 400$ Myr,

² Hereafter we denote indistinguishably the bulge and the central 500 pc region of the galaxy, which for an exponentially-decreasing spherically-symmetric profile with 200 pc scale radius (the value at $t = 1$ Gyr) corresponds to the radius that contains 50 per cent of the mass.

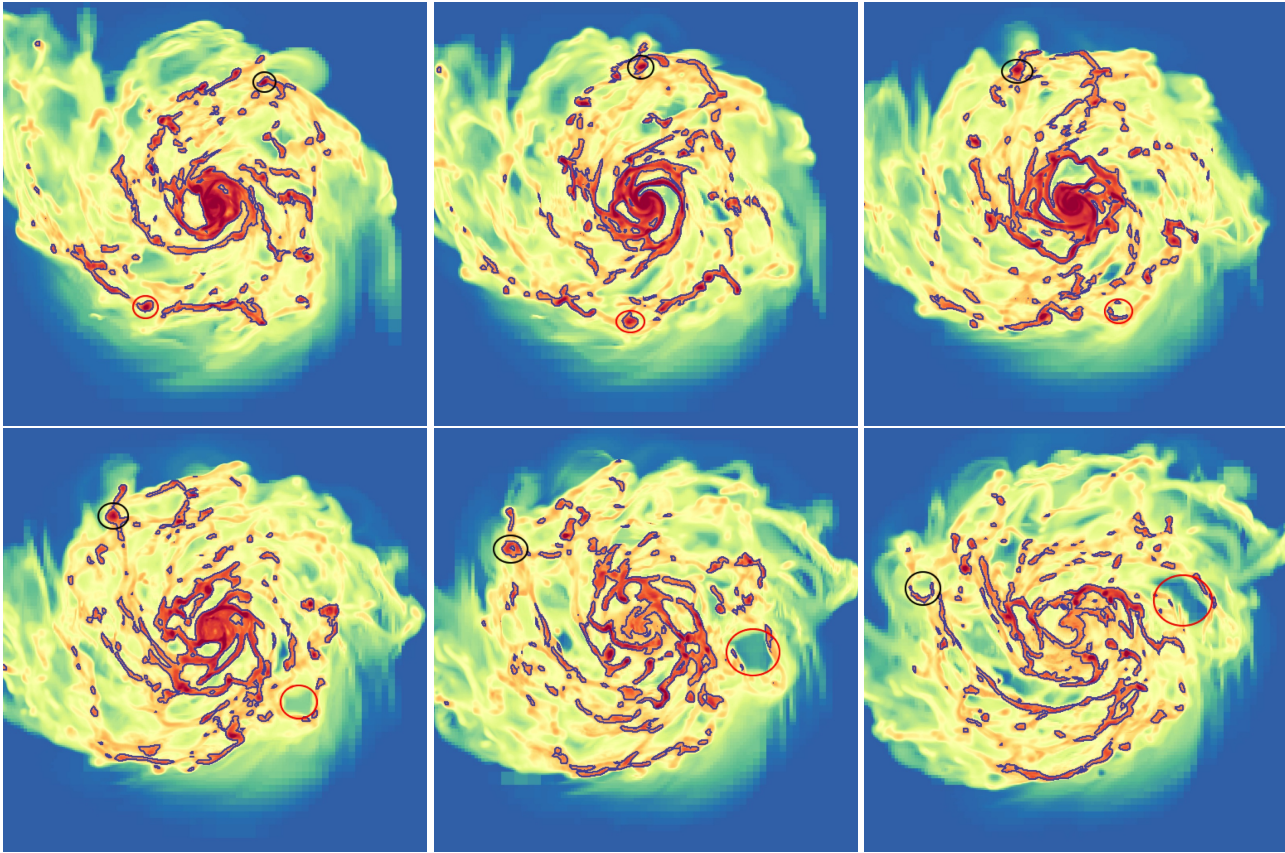


Figure 3. Isolated galaxy simulation. Time sequence of the gas density seen face-on at $t = 610$ Myr from top left to bottom right, each snapshot is separated by 2 Myr. Image size is 5 kpc. This time sequence highlights the short-lived nature of small-scale substructures in the ISM. The colour table is from 0.1 H cm^{-3} (blue) to 10^4 H cm^{-3} (red). The blue contours surround the regions of star formation with gas density above 250 H cm^{-3} . Note the decrease in the gas density in the bulge of the galaxy. Two gas clumps are identified in the outskirts of the galaxy (black and red circles), which are destroyed by the SN explosions.

when the activity of the SFR has decreased, small SNe bubbles rise a few hundred parsecs above the disc plane similar to what is observed in our own Milky Way disc (see bottom panel of Fig. 2).

In the disc, SFR and, thus, SNe feedback, are strongly clustered in small star-forming regions, where gas reaches densities above 250 H cm^{-3} , and, in turn, strong localized feedback periodically disrupts the cold clumps of gas that are the nursery of stars. This behaviour is illustrated in Fig. 3 with a time sequence of the gas density in the disc where two dense clumps of gas are pinpointed. After a typical time of $t_{\text{SN}} = 10$ Myr that corresponds to the average time for type II SNe to explode after the formation of the stellar particle, the whole clump is dispersed into the diffuse ISM. Such clustered explosions naturally force the continuous driving of turbulence and the mixing of the various, hot/diffuse and cold/dense, phases of the ISM. The same process happens in the bulge region where the star-forming gas is more extended. The gas component is in the form of a compact disc exhibiting small spiral arms and after some time the whole region is dispersed by the heating of SNe feedback, increasing turbulence and therefore the overall velocity dispersion of the gas.

We recall that the formation and rapid destruction of large-density clumps is the direct consequence of the

adopted scheme for SNe feedback using delayed cooling. This implementation is designed to affect the formation of such regions without radiating any of the thermal energy up to the point where the blast wave has propagated over a Jeans length. Less efficient SN feedback implementations such as the one from Dubois & Teyssier (2008) allow for the long term survival of such clumps, and the consequences on the central BH growth is investigated in detail in paper I.

4.1.2 Evolution of the BH mass and spin

Now that we have shown how SNe feedback alone is able to constantly reprocess the cold gas material in the ISM, we can investigate the growing mode of the central BH and in particular the evolution of its spin with respect to the accretion and gas dynamics.

Fig. 1 shows the evolution of the BH mass with time. The BH starts with an initial seed mass of $10^4 M_{\odot}$ and grows up to $M_{\text{BH}} \simeq 3 \times 10^5 M_{\odot}$ after 1 Gyr. It is apparent that the BH has not spent much time accreting at the Eddington limit; $\chi = (10^3/t_{\text{salp}}) \ln(M_{\text{BH}}/10^4 M_{\odot}) = 0.2 - 0.6$ respectively assuming a Salpeter time-scale of $t_{\text{salp}} = 45$ Myr ($\epsilon_r = 0.1$) or $t_{\text{salp}} = 135$ Myr ($\epsilon_r = 0.32$). Also the BH does not seem to have reached the state where its own feedback is sufficient to self-regulate its mass growth as it grows in

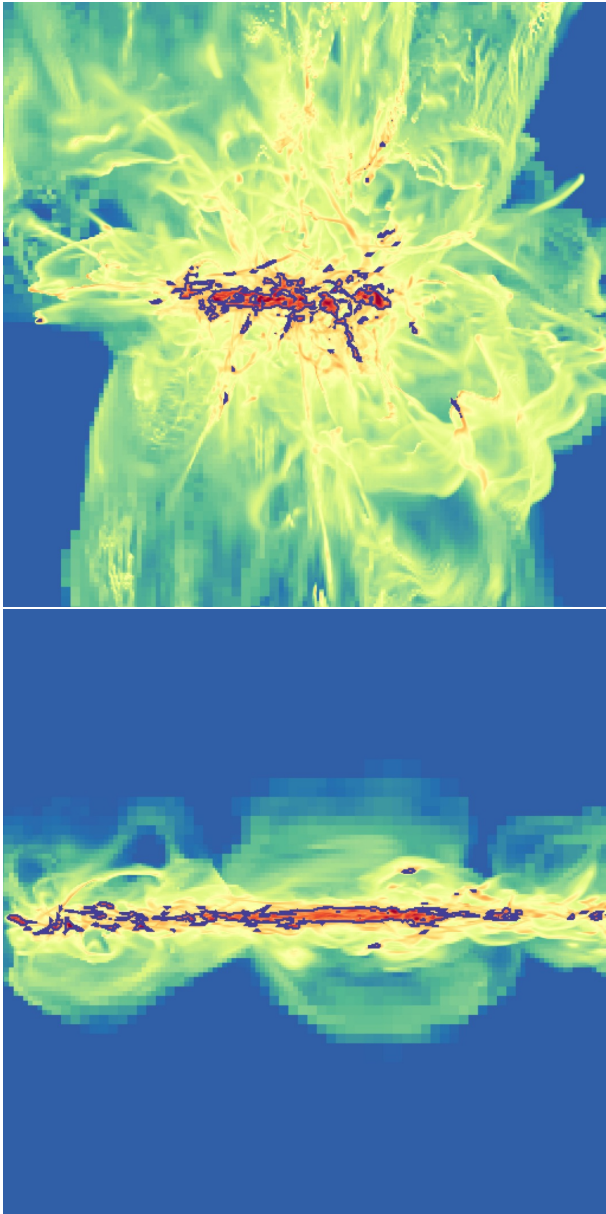


Figure 2. Isolated galaxy simulation. Edge-on view of the gas density of the galaxy at $t = 250$ Myr (top) and $t = 1000$ Myr (bottom). Image size is 5 kpc. The colour table is from 0.1 H cm^{-3} (blue) to 10^4 H cm^{-3} (red). The blue contours surround the regions of star formation with gas density above 250 H cm^{-3} . At early times, the strong activity of star formation produces large-scale outflows that rise up to 5 kpc above the disc and fall back into a galactic fountain. At late times, the more quiescent activity leads to the formation of hot bubbles of a few 100 pc size.

mass over large time extents. This is partially explained by the fact that the BH growth shows multiple rapid increases in mass followed by a plateau (similar to how the stellar mass grows in time). The form of this curve is the direct consequence of SNe feedback creating outflows in the bulge and removing the cold gas that corresponds to the plateau of periods of low star-formation activity within that region of the galaxy.

The spin evolution of the BH in Fig. 4 does not show any large variation. The value of the spin is always above

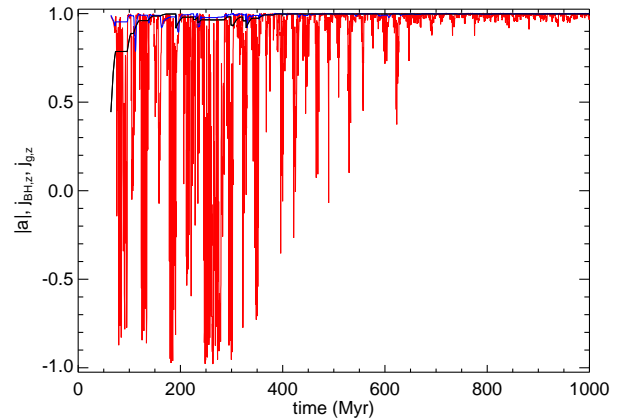


Figure 4. Isolated galaxy simulation. BH spin (black), vertical component of the BH AM (blue) and of the accreted gas AM (red) as a function of time over the whole run. The BH spin magnitude is always very large due to synchronisation between the BH spin direction and that of accreted gas AM during the phases of rapid growth, driven by cold, rotationally supported gas.

$|a| > 0.9$ after the first e-folding time-scale of the BH growth. We see some variations of the order of $\delta a = 0.1$ but, soon after, accretion is strong enough to rapidly re-align gas and BH spin, and bring the spin of the BH back to $|a| > 0.9$. Recall that if accretion is completely random in terms of AM direction (and constant in accretion rate), the spin of the BH would be close to zero as a BH gets spun down faster than it is spun up. Conversely, if accretion is coherent in AM direction, or at least has some level of coherence (Dotti et al. 2013), the BH keeps very high spin values.

The reason for this large value of the BH spin has to do with both the orientation of the gas in the surroundings and the synchronisation with events of strong accretion driven by cold and dense gas. The blue curve of Fig. 4 shows that the direction of the BH AM is always pointing towards the vertical direction and is, thus, well aligned with the galactic AM. The red curve shows instead the z-direction of the AM of the gas accreted onto the BH (red curve in Fig. 4). During the galactic fountain phase (< 400 Myr), this direction can be rapidly changing, while at a later stage, when the galactic fountain is replaced by low-rising bubbles, the gas AM realigns with the vertical direction of the disc.

If the direction of the accreted gas AM is quickly changing in the galactic fountain phase, why is the BH spin unaffected? A careful inspection of such “chaotic” events is shown in Fig. 5. Some time intervals with opposite accreted gas AM and BH AM are clearly identified, such as at $245 < t < 285$ Myr, and should, in principle, decrease the BH spin. However, this prolonged chaotic period is also synchronised with a period of extremely low accretion rate onto the BH, $\dot{M}_{\text{BH}} \ll \dot{M}_{\text{Edd}}$, so that the BH does not accrete enough gas to decrease durably and significantly its spin amplitude. *Vice versa*, prolonged high-accretion rates onto the BH, $\dot{M}_{\text{BH}} \sim \dot{M}_{\text{Edd}}$, correspond to accreted gas AM aligned with both the BH AM and the galactic disc (with the vertical axis). The sustained BH accretion events are driven by the replenishing of the cold, dense gas reservoir in the bulge of the galactic disc, which is also synchronised

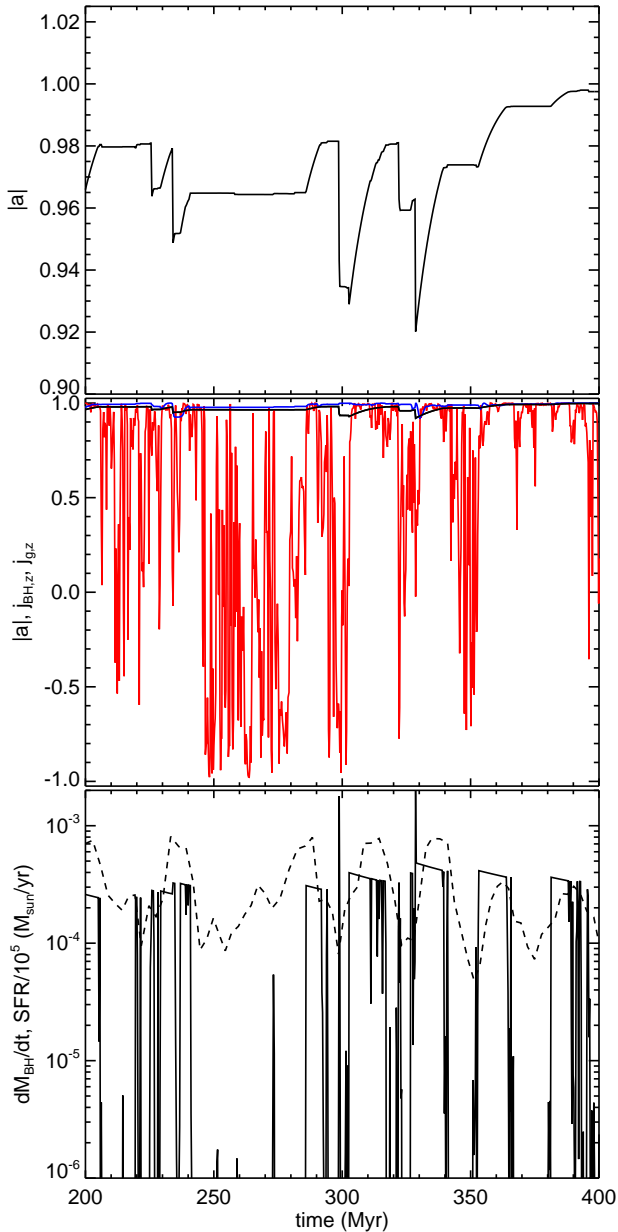


Figure 5. Isolated galaxy simulation. *Top panel:* Spin as a function of time. *Middle panel:* BH spin (black), vertical component of the BH AM (blue) and of the accreted gas AM (red) as a function of time. *Bottom panel:* BH accretion rate (solid), SFR within the $r < 500$ pc bulge of the galaxy (dashed, in $10^5 M_{\odot} \text{yr}^{-1}$ units) as a function of time for 200 Myr of evolution, to highlight the short-term variability.

with the peak of the SFR, and in that case the whole central region co-rotates with the galactic disc.

The BH grows for the most part accreting smooth gas rather than clumps. The accretion of clumps is limited because these clumps have extremely short life-times (~ 10 Myr) and most of them can not reach the bulge before being destroyed by SNe. In the case where clumps are more long-lived, the situation could be different. This alternative scenario has been tested in Appendix A of Dubois

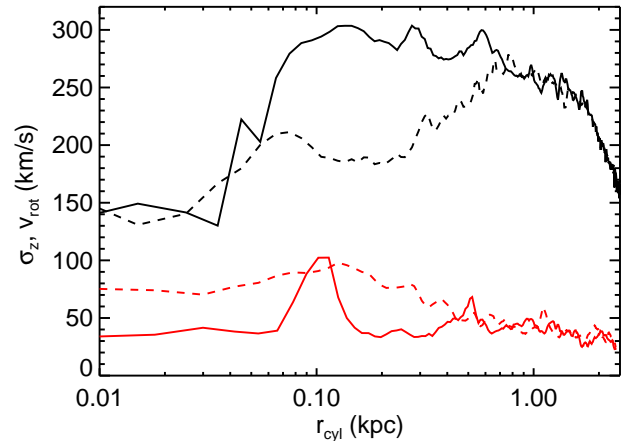


Figure 6. Rotational velocity (black) and vertical velocity dispersion (red) of the dense gas as a function of cylindrical radius at two different times $t = 612$ Myr when the BH accretes at Eddington (solid line) and at $t = 620$ Myr when the accretion rate on the BH becomes negligible (dashed line). These times correspond to the top right and bottom right images of Fig. 3 respectively. Low accretion onto the BH happens when the velocity dispersion of the gas close to the BH increases. In phases of strong gas accretion, coherent gas rotation dominates over random motions in the gas.

et al. (2013), and is reproduced in the Appendix B of the current paper, with inefficient SNe feedback (long-lived star-forming clouds), and we found that even though the BH can grow by the capture of gas clumps (especially at late times), the gas AM of the accreted clumps is typically well-aligned with that of the underlying gas disc.

In Fig. 6 we show the vertical velocity dispersion of the dense gas with $n > 1 \text{ H cm}^{-3}$ at two different times when the BH accretes at Eddington corresponding to the top right panel of Fig. 3, and when the accretion drops below $10^{-3} M_{\text{Edd}}$ corresponding to the bottom right panel. The gas velocity dispersion and rotational velocity in the central region, very close to the BH, are of comparable value, with 150 km s^{-1} for the rotational velocity, and 40 and 70 km s^{-1} for the velocity dispersion respectively before and while the gas is blown away from the centre due to SNe energy release. Outside the very centre, the gas rotational velocity increases up to $v_{\text{rot}} \simeq 250 \text{ km s}^{-1}$ and the gas velocity dispersion goes to $\sigma_z \simeq 50 \text{ km s}^{-1}$. We also clearly see the effect of the SNe energy release in the velocity patterns, both in the rotation of the gas and in the velocity dispersion in the $50 < r_{\text{cyl}} < 500$ pc radius range: SNe explosions temporarily increase the velocity dispersion of the gas, while they reduce the velocity rotation. The fact that the gas velocity dispersion does not overwhelm the gas motion near the BH explains why the BH spin keeps very large values and is consistently pointing towards the same direction, which is the one of the gas AM around the BH.

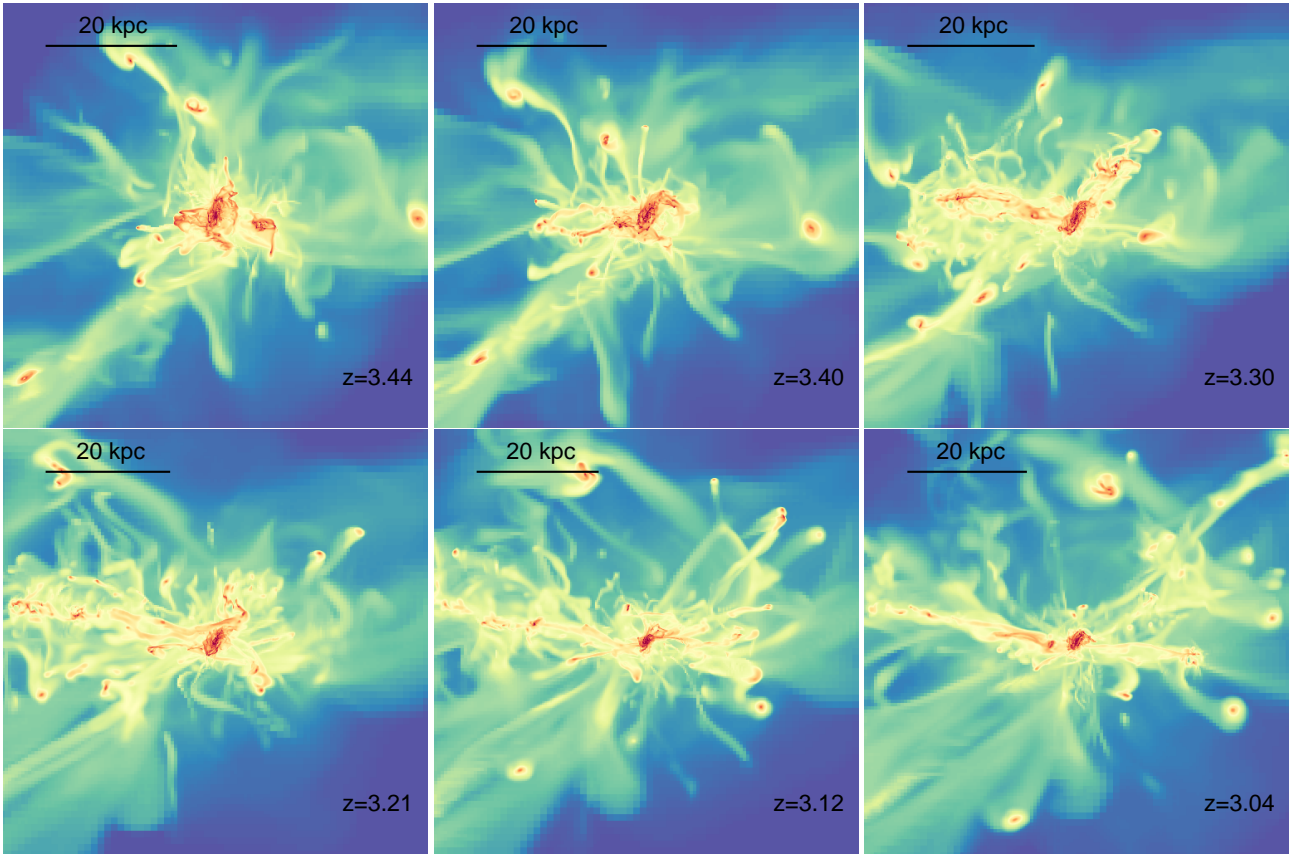


Figure 9. SETH cosmological zoom simulation. Projected gas density at different redshifts illustrating the merger of one gas-rich satellite with the central galaxy. The colour table is from $10^{-3} \text{ H cm}^{-3}$ (blue) to 10^2 H cm^{-3} (red). The virial radius of the underlying dark matter halo is $\simeq 50 \text{ kpc}$. Some dense filamentary gas is stripped out during the head-on collision and falls back onto the galaxy.

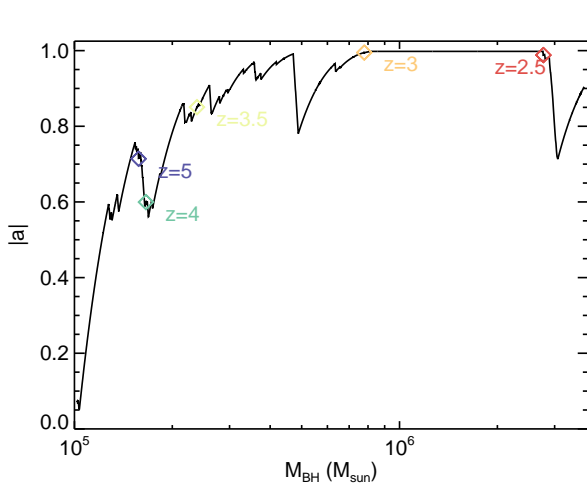


Figure 7. SETH cosmological zoom simulation. Spin magnitude versus mass for the BH of the central most massive galaxy. Different values of redshift are indicated with diamonds. The spin grows to its maximum value at $z \sim 3$, and then remains above 0.7.

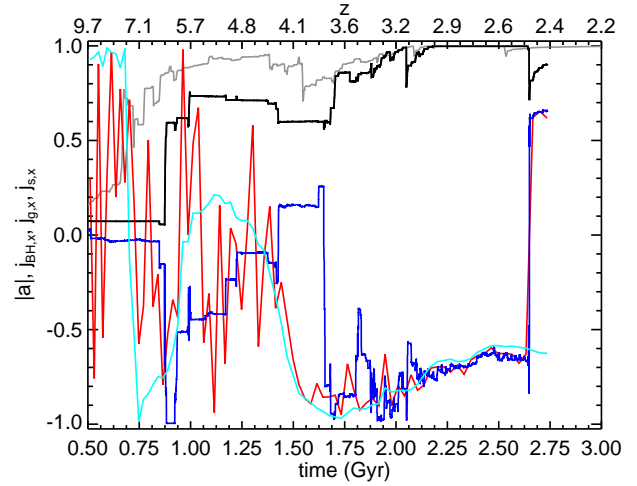


Figure 8. SETH cosmological zoom simulation. Magnitude of the BH spin (black), x-component of the gas AM within 500 pc (red) of the BH spin (blue) and of the stars within the galaxy (cyan) as a function of time and redshift. The light grey line is for the SETH low-resolution simulation with $\Delta x = 40 \text{ pc}$. At early stages ($\sim 1.5 \text{ Gyr}$), the gas behaviour is chaotic and shows large fluctuations of the AM direction. At later times, gas settles in the galaxy and there is a strong persistent correlation between the BH spin, the gas AM and that of the stars in the galaxy, which leads to relatively high spin values.

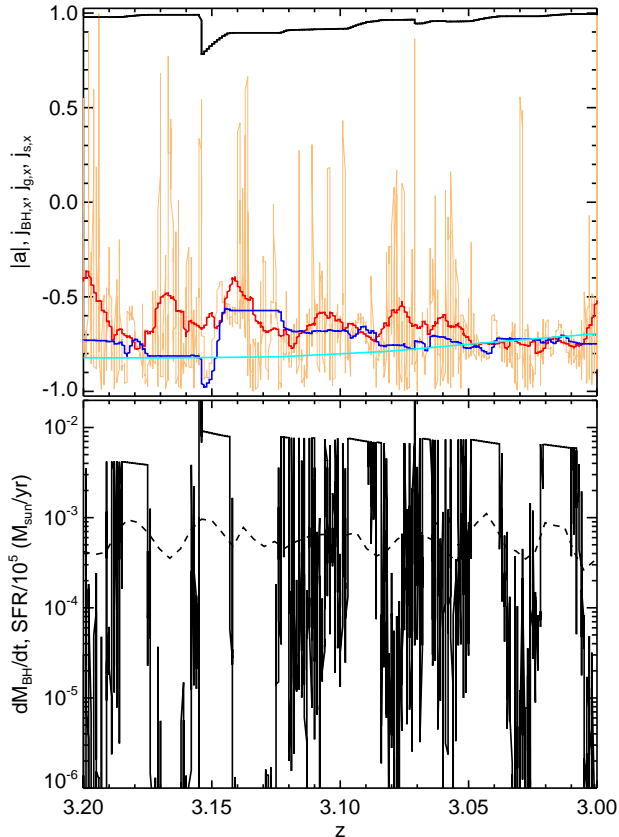


Figure 10. SETH cosmological zoom simulation. *Top panel:* Absolute value of the BH spin versus redshift (black), x-component of the accreted gas AM (instantaneous in orange and smoothed in red), of the spin (blue) and of the stars within the galaxy (cyan). *Bottom panel:* BH mass accretion rate (solid) and SFR/ $10^5 M_{\odot}$ (dashed). Eddington-limited accretion episodes are synchronous with a strong correlation between the directions of the accreted gas AM, the BH spin and the galactic AM.

4.2 The SETH simulation: a cosmological laboratory for BH spin evolution

As discussed in Paper I, the resolution employed in SETH allows us to resolve the multiphase structure of the galaxy with star-forming clumps of dense cold gas, hotter diffuse gas. At relatively late cosmic times, $z < 3.5$, it also allows us to identify the formation of a razor thin disc of stars, a hotter and thicker disc of stars, and old clusters of stars flying around the galactic disc. At earlier epochs though, the galaxy’s disc has not settled, as the gas is constantly stirred and reprocessed by the efficient feedback from SNe. The gravitational potential of the galaxy and of the host halo is not deep enough to prevent the galactic wind from escaping and gas rarely condenses in the central region close to the BH. Above $z > 3.5$ the growth of the BH is very slow, as shown in Fig. 7: BH growth is delayed and the mass of the BH only increases by a factor 2. When galaxy and halo have grown sufficiently, their gravitational potential is able to retain the gas affected by SN feedback and a gaseous disc finally forms (around $z \sim 3.5$). Cold gas starts to accumulate within the central region around the BH. Since this gas

originates from the recently settled disc, the AM of the gas that feeds the BH tends to have a coherent AM direction.

Fig. 8 shows that above $z > 3.5$ (before $t < 1.8$ Gyr) the magnitude of the BH spin is initially constant over long timescales, while the accretion rate on the BH is small, and spin changes only when a gas clump approaches. In this phase the gas AM in the central region (500 pc) is randomly oriented because SNe explosions easily eject gas out of the galaxy, precluding the settling of a persistent gas disc. The accreted gas AM - not represented in Fig. 8 - shows an even more chaotic behaviour early on, with sudden variations from one coarse time step to another. Once the gas in the galaxy starts to settle in a rotationally supported disc (below $z < 3.5$), because SNe become unable to eject gas out of the galaxy, the BH spin starts increasing, until it reaches its maximum magnitude at $z \sim 3$. Meanwhile, the accreted gas AM becomes coherent in time and well aligned with the BH spin direction and that of the AM of the galaxy (defined here as the AM of the stars).

Several external perturbations caused by satellites flying around the halo are observed at any redshift. There is one particular event where a gas-rich merger produces a large ejection of gas from the central galaxy into the circum-galactic medium (Fig. 9). A gas-rich satellite galaxy at $z = 3.44$ collides with the central one head-on, passing through the galactic disc and stripping gas. When this cold (a few 10^4 K) moderately-dense (a few 0.1 H cm^{-3}) gas falls back onto the galaxy, it is misaligned with the original gas AM. When this gas reaches the BH, it triggers accretion of counter-rotating material and the spin magnitude decreases as shown in Fig. 10 at $z = 3.15$.

Towards the end of the simulation, $t = 2.65$ Gyr ($z = 2.5$), the accreted gas AM suddenly counter-rotates with respect to both the BH spin and stellar AM. This is caused by a large-scale cold gas filament which swaps sides in its connection to the galaxy, all of a sudden providing its AM in the opposite direction (an effect already outlined in Tillson et al. 2012). This event decreases the spin amplitude, but the direction of the BH spin eventually re-aligns with the direction of the gas AM before the spin down process is completed (Dotti et al. 2013). Note that the result is not extremely sensitive to a change in spatial resolution: for the SETH simulation with $\Delta x = 40$ pc resolution the BH spin grows slowly to large values at early times, and keeps a value close to 1 when the disc is settled, while gas-rich mergers and counter-rotating cosmic filamentary accretion are decreasing the value of the spin at almost the same positions in time (see Fig. 8).

As for the isolated galaxy simulation, the BH growth is episodic with short bursts of accretion at or close to the Eddington limit, followed by periods of negligible accretion ($\dot{M}_{\text{BH}} < 10^{-3} M_{\odot}$) as we can observe in Fig. 10. The Eddington-limited accretion events are synchronous with the peaks of the star formation rate in the galaxy and, in particular, with the peaks of the SFR in the bulge, when cold dense gas is present around the BH.

The same figure (Fig. 10) also displays the direction of the BH spin, accreted gas and galaxy AM with respect to a fixed reference frame. They are all very coherent over time, all pointing towards the same direction and with very little variation. The direction of the accreted gas AM is *on average* pointing in the same direction during long extended period

of times (red curve), while it *instantaneously* swings because of the efficient feedback produced by local SN explosions. However, since these explosions inject energy in the cold, dense gas, transforming it into diffuse and hot material, accretion onto the BH drops to extremely low values and these chaotic periods cannot effectively spin down the BH. Note also the slight drift of the galaxy AM (stellar component) over time which is the result of smooth torques exerted by the external perturbations (cold streams, diffuse accretion of gas, minor mergers), while at some very specific moments the spin of the galaxy changes due to more significant mergers (e.g. at $z = 5.9$ and $z = 4.3$, see Fig. 7).

5 CONCLUSIONS AND DISCUSSION

By means of high-resolution hydrodynamical simulations, we have followed the SN driven reprocessing of cold star-forming gas into a hot diffuse interstellar medium and its effect on the evolution of the spin of central supermassive BH. All these physical quantities were evolved on-the-fly in a self-consistent manner. The turbulence induced by stellar feedback is described by ‘maximal’ model, to highlight its impact on the angular momentum of the gas accreted by the BH. With two different kinds of initial conditions: an isolated collapsing halo and a zoomed cosmological halo evolved for several hundreds of Myrs, we reach similar conclusions. SN-driven turbulence does not contribute to randomising the angular momentum of the gas effectively accreted by the BH. This is because the BH grows in mass by accreting cold, dense gas, which tends to reside in a rotationally supported disc. The gas made turbulent by SN energy injection is instead hot and diffuse and hardly contributes to the BH evolution. The accretion of the cold star-forming gas onto the central BH adds constructively in terms of angular momentum, and over time increases the BH spin to high values even though the turbulence in the ISM is as large as 50 km s^{-1} .

When SN feedback activity is at minimum, the mass growth of the BH and its spin evolution are driven by Eddington-limited phases where the gas around the BH is dense and its rotation is imposed by the global rotation of the galactic disc. The phases of random chaotic accretion that could efficiently lower the BH spin are synchronous with periods of SNe explosions that quench the accretion rate onto the BH by creating low-density and hot expanding bubbles.

The cosmological perturbations induced by galaxy mergers and cold filaments can significantly alter the AM of gas in the galaxy and the accretion flow on the BH, reorient the direction of the spin, and lower its value. However, these events are sufficiently rare and short in duration, even at high redshift, that the BH spin rapidly returns to its steady-state, maximal value through accretion of this fresh ISM gas.

The large values of the spin measured in these simulations for gas-rich galaxies have potentially severe consequences on the growth of high-redshift supermassive BH as observed in the SDSS (e.g. Fan & et al., 2006). Indeed, the characteristic time-scale for the growth of BH is inversely proportional to the radiative efficiency of the accretion process, which, for radiatively efficient accretion discs, is an

increasing function of the BH spin. For a radiative efficiency of $\epsilon_r = 0.1$, a value commonly used in cosmological simulations (Sijacki et al. 2007; Di Matteo et al. 2008; Booth & Schaye 2009; Dubois et al. 2012) and in agreement with Soltan’s argument, the e-folding Salpeter time is $t_{\text{salp}} = 45 \text{ Myr}$, meaning that BH can grow as large as $10^9 M_\odot$ within 1 Gyr ($z = 6$) even when starting from large stellar seed mass values ($10^2 - 10^3 M_\odot$). For BH spinning with values $a = 0.998$ as in our simulations, the radiative efficiency and the Salpeter time become $\epsilon_r = 0.32$ and $t_{\text{salp}} = 135 \text{ Myr}$. Thus, a maximally spinning BH cannot reach $10^9 M_\odot$ in less than a Gyr if its accretion is Eddington-limited. One simple way to solve this apparent mismatch is that BH grow at super-Eddington rates (e.g., Volonteri & Rees 2005). Super-Eddington accretion alleviates the time-scale constraint provided that there is enough gas in the very centre of galaxies early on, which seems to be the case (Dubois et al. 2012). At the same time, in radiatively inefficient super-Eddington accretion discs (e.g., slim discs, but note that this is true for the case of very sub-Eddington flows as well) there is no expectation that the radiative efficiency strongly depends on BH spin, at variance with mildly sub-Eddington radiatively efficient discs, such as Shakura-Sunyaev discs.

ACKNOWLEDGMENTS

The simulations presented here were run on the DiRAC-1 and DiRAC-2 facilities jointly funded by STFC, the Large Facilities Capital Fund of BIS and the Universities of Oxford and Leicester. This research is part of the Horizon-UK project. This research has been supported in part by the International Balzan Foundation via New College, Oxford, and by the National Science Foundation under Grant No. NSF PHY11-25915. YD and JS acknowledge support by the ERC advanced grant (Dark Matters). MV acknowledges funding support from NASA, through award ATP NNX10AC84G, and from a Marie Curie Career Integration grant (PCIG10-GA-2011-303609).

References

- Baker J. G., Boggs W. D., Centrella J., Kelly B. J., McWilliams S. T., Miller M. C., van Meter J. R., 2007, *ApJ*, 668, 1140
- Bardeen J. M., 1970, *Nature*, 226, 64
- Bardeen J. M., Petterson J. A., 1975, *ApJ Let.*, 195, L65
- Bellovary J., Brooks A., Volonteri M., Governato F., Quinn T., Wadsley J., 2013, *ApJ*, 779, 136
- Bondi H., 1952, *MNRAS*, 112, 195
- Booth C. M., Schaye J., 2009, *MNRAS*, 398, 53
- Bournaud F., Dekel A., Teyssier R., Cacciato M., Daddi E., Juneau S., Shankar F., 2011, *ApJ Let.*, 741, L33
- Bournaud F. et al., 2013, ArXiv e-prints
- Bower R. G., Benson A. J., Malbon R., Helly J. C., Frenk C. S., Baugh C. M., Cole S., Lacey C. G., 2006, *MNRAS*, 370, 645
- Bullock J. S., Dekel A., Kolatt T. S., Kravtsov A. V., Klypin A. A., Porciani C., Primack J. R., 2001, *ApJ*, 555, 240

- Campanelli M., Lousto C., Zlochower Y., Merritt D., 2007a, *ApJ Let.*, 659, L5
- Campanelli M., Lousto C. O., Zlochower Y., Merritt D., 2007b, *Physical Review Letters*, 98, 231102
- Chapon D., Mayer L., Teyssier R., 2013, *MNRAS*, 429, 3114
- Croton D. J. et al., 2006, *MNRAS*, 365, 11
- Dexter J., Fragile P. C., 2011, *ApJ*, 730, 36
- Di Matteo T., Colberg J., Springel V., Hernquist L., Sijacki D., 2008, *ApJ*, 676, 33
- Di Matteo T., Khandai N., DeGraf C., Feng Y., Croft R. A. C., Lopez J., Springel V., 2012, *ApJ Let.*, 745, L29
- Di Matteo T., Springel V., Hernquist L., 2005, *Nature*, 433, 604
- Dotti M., Colpi M., Pallini S., Perego A., Volonteri M., 2013, *ApJ*, 762, 68
- Dubois Y., Devriendt J., Slyz A., Teyssier R., 2010, *MNRAS*, 409, 985
- Dubois Y., Devriendt J., Slyz A., Teyssier R., 2012, *MNRAS*, 420, 2662
- Dubois Y., Pichon C., Devriendt J., Silk J., Haehnelt M., Kimm T., Slyz A., 2013, *MNRAS*, 428, 2885
- Dubois Y., Pichon C., Haehnelt M., Kimm T., Slyz A., Devriendt J., Pogosyan D., 2012, *MNRAS*, 423, 3616
- Dubois Y., Teyssier R., 2008, *A&A*, 477, 79
- Dubois Y., Volonteri M., Devriendt J., Slyz A., Silk J., 2013, ArXiv e-prints
- Dubois Y., Volonteri M., Silk J., 2013, ArXiv e-prints
- Fan X., et al., 2006, *AJ*, 132, 117
- Feng Y., Di Matteo T., Croft R., Khandai N., 2013, ArXiv e-prints
- Fragile P. C., Anninos P., 2005, *ApJ*, 623, 347
- Fragile P. C., Blaes O. M., Anninos P., Salmonson J. D., 2007, *ApJ*, 668, 417
- Gabor J. M., Bournaud F., 2013, *MNRAS*, 434, 606
- Gammie C. F., Shapiro S. L., McKinney J. C., 2004, *ApJ*, 602, 312
- Goodman J., Tan J. C., 2004, *ApJ*, 608, 108
- Haardt F., Madau P., 1996, *ApJ*, 461, 20
- Hahn O., Abel T., 2011, *MNRAS*, 415, 2101
- Häring N., Rix H.-W., 2004, *ApJ Let.*, 604, L89
- Hopkins P. F., Hernquist L., Hayward C. C., Narayanan D., 2012, *MNRAS*, 425, 1121
- Jiang L., et al., 2009, *AJ*, 138, 305
- Johnson J. L., Whalen D. J., Li H., Holz D. E., 2013, *ApJ*, 771, 116
- Kennicutt Jr. R. C., 1998, *ApJ*, 498, 541
- King A., 2003, *ApJ Let.*, 596, L27
- King A. R., Lubow S. H., Ogilvie G. I., Pringle J. E., 2005, *MNRAS*, 363, 49
- King A. R., Pringle J. E., Hofmann J. A., 2008, *MNRAS*, 385, 1621
- King A. R., Pringle J. E., Livio M., 2007, *MNRAS*, 376, 1740
- Kolykhalov P. I., Syunyaev R. A., 1980, *Soviet Astronomy Letters*, 6, 357
- Krumholz M. R., Tan J. C., 2007, *ApJ*, 654, 304
- Kulier A., Ostriker J. P., Natarajan P., Lackner C. N., Cen R., 2013, ArXiv e-prints
- Libeskind N. I., Cole S., Frenk C. S., Helly J. C., 2006, *MNRAS*, 368, 1381
- Magorrian J. et al., 1998, *AJ*, 115, 2285
- Maio U., Dotti M., Petkova M., Perego A., Volonteri M., 2013, *ApJ*, 767, 37
- Moderski R., Sikora M., 1996a, *A&A*, 120, C591
- Moderski R., Sikora M., 1996b, *A&A*, 120, C591
- Moderski R., Sikora M., Lasota J.-P., 1998, *MNRAS*, 301, 142
- Mortlock D. J., et al., 2011, *Nature*, 474, 616
- Natarajan P., Pringle J. E., 1998, *ApJL*, 506, L97
- Navarro J. F., Frenk C. S., White S. D. M., 1997, *ApJ*, 490, 493
- Nelson R. P., Papaloizou J. C. B., 2000, *MNRAS*, 315, 570
- Ogilvie G. I., 1999, *MNRAS*, 304, 557
- Omma H., Binney J., Bryan G., Slyz A., 2004, *MNRAS*, 348, 1105
- Ostriker E. C., 1999, *ApJ*, 513, 252
- Papaloizou J. C. B., Pringle J. E., 1983, *MNRAS*, 202, 1181
- Perego A., Dotti M., Colpi M., Volonteri M., 2009, *MNRAS*, 399, 2249
- Planck Collaboration et al., 2013, ArXiv e-prints
- Powell L. C., Slyz A., Devriendt J., 2011, *MNRAS*, 414, 3671
- Pringle J. E., 1981, *ARA&A*, 19, 137
- Rees M. J., 1978, *Nature*, 275, 516
- Reynolds C. S., 2013, *SSR*
- Rezzolla L., Barausse E., Dorband E. N., Pollney D., Reisswig C., Seiler J., Husa S., 2008, *Phys. Rev. D*, 78, 044002
- Sądowski A., Bursa M., Abramowicz M., Kluźniak W., Lasota J.-P., Moderski R., Safarzadeh M., 2011, *A&A*, 532, A41
- Scheuer P. A. G., Feiler R., 1996a, *MNRAS*, 282, 291
- Scheuer P. A. G., Feiler R., 1996b, *MNRAS*, 282, 291
- Shakura N. I., Sunyaev R. A., 1973, *A&A*, 24, 337
- Sijacki D., Springel V., Di Matteo T., Hernquist L., 2007, *MNRAS*, 380, 877
- Sijacki D., Springel V., Haehnelt M. G., 2011, *MNRAS*, 414, 3656
- Silk J., Rees M. J., 1998, *A&A*, 331, L1
- Sorathia K. A., Krolik J. H., Hawley J. F., 2013, *ApJ*, 777, 21
- Sorathia K. A., Krolik J. H., Hawley J. F., 2013, *The Astrophysical Journal*, 768, 133
- Springel V., 2005, *MNRAS*, 364, 1105
- Stinson G., Seth A., Katz N., Wadsley J., Governato F., Quinn T., 2006, *MNRAS*, 373, 1074
- Sutherland R. S., Dopita M. A., 1993, *ApJ Sup.*, 88, 253
- Tasker E. J., 2011, *ApJ*, 730, 11
- Teyssier R., 2002, *A&A*, 385, 337
- Teyssier R., Moore B., Martizzi D., Dubois Y., Mayer L., 2011, *MNRAS*, 414, 195
- Teyssier R., Pontzen A., Dubois Y., Read J. I., 2013, *MNRAS*, 429, 3068
- Thorne K. S., 1974, *ApJ*, 191, 507
- Tillson H., Devriendt J., Slyz A., Miller L., Pichon C., 2012, ArXiv e-prints
- Tremaine S. et al., 2002, *ApJ*, 574, 740
- Volonteri M., Gültekin K., Dotti M., 2010, *MNRAS*, 404, 2143
- Volonteri M., Madau P., 2008, *ApJ Let.*, 687, L57
- Volonteri M., Rees M. J., 2005, *ApJ*, 633, 624
- Volonteri M., Sikora M., Lasota J.-P., 2007, *ApJ*, 667, 704
- Wyithe J. S. B., Loeb A., 2003, *ApJ*, 595, 614
- Yu Q., Tremaine S., 2002, *MNRAS*, 335, 965

APPENDIX A: RESOLUTION STUDY

In this section, we test how the results depend on the simulations’ resolution, by changing the minimum cell size (maximum level of refinement) in the isolated galaxy run. We performed three simulations at lower resolution $\Delta x = 20, 40$ and 80 pc. In the three additional runs the density threshold for star formation in the polytropic EoS, $n_0 = 62.5, 15.5$ and 4 H cm^{-3} , and the dissipation time-scale of the non-thermal component for SNe feedback $t_{\text{diss}} = 0.95, 2.41$ and 4.82 Myr scale with the resolution. These parameters are calibrated to keep the propagation length of the blast wave constant in number of resolution elements ($\lambda_{\text{Jeans}} = 4\Delta x$) for explosions occurring at $n = n_0$.

Projections of the face-on and edge-on gas densities are shown in Fig. A1 after 800 Myr of evolution. As expected, the small-scale structure of the ISM is smoothed out with decreasing resolution. Large-scale features such as gas concentrations in the central region, spiral arms of gas and 100 pc SNe-driven bubble are however observed in all four runs with different resolutions. The consequence is that the average star formation rates are similar $\langle SFR \rangle \simeq 20 M_{\odot} \text{ yr}^{-1}$ but the bursts appear at different times and with different amplitudes (left panel of Fig. A2). As the details of star formation change, the fuelling of the central BH differ and the central supermassive BH has a slightly different mass growth and spin evolution. However, the final BH masses end up with similar values between $1\text{--}3 \times 10^6 M_{\odot}$ (middle panel of Fig. A2) and similar values of the spin are observed in all runs, with $|a| \gtrsim 0.8$ (right panel of Fig. A2). This resolution study shows that BHs grow at about Eddington with large spin values independently of how much the multiphase structure of the ISM is resolved.

APPENDIX B: A DIFFERENT MODELING OF SUPERNOVA FEEDBACK

In this Appendix, we present the result of the isolated galaxy simulation with $\Delta x = 10$ pc and a different scheme for SN feedback described in Dubois & Teyssier (2008). This feedback modelling is based on a kinetic approach where mass, momentum and energy are released in the immediate vicinity of the exploding stellar particle, and cooling takes place everywhere and at all times, i.e. independently of whether recent explosions have occurred in a specific place or not. With this approach, SN feedback becomes effective only in diffuse regions of the ISM, as energy is quickly thermalised and radiated away when the explosions take place in cold dense clouds. As a consequence, star-forming clouds are long-lived structures, until they consume all their gas into stars or are captured by the central bulge. Tasker (2011) have shown that amongst the large variety of star-forming clouds in Toomre unstable discs, there are co- and counter-rotating clumps (with a preference for co-rotating clumps).

Therefore, with that feedback implementation, the cold gas feeds the central BH in a coherent fashion up to the point where this BH gets massive enough to self-regulate and blow away the gas in its immediate vicinity. Once the self-regulated state is achieved, only the cold star-forming clouds that manage to reach the very centre of the galaxy trigger episodes of massive fuelling of the BH (Bournaud et al.

2011; Dubois et al. 2012, 2013,?; Gabor & Bournaud 2013; Bournaud et al. 2013).

APPENDIX C: SPIN ALIGNMENT TIMESCALES

The timescale over which BH spins align with the angular momentum of the accretion flow, and its relation to the accretion timescale have been the subject of a long debate for decades (e.g., Bardeen & Petterson 1975; Rees 1978; Papaloizou & Pringle 1983; Scheuer & Feiler 1996b; Natarajan & Pringle 1998; Nelson & Papaloizou 2000; Fragile & Anninos 2005; Fragile et al. 2007; Dexter & Fragile 2011; Sorathia et al. 2013; Sorathia et al. 2013). In this Appendix we explore the consequences of alignment timescales longer than assumed in the main article, and we test how sensitive the results are to the accretion rate behaviour and its synchronisation with gas cooling. We analyse the isolated galaxy run, and we post-process the relative BH alignment and spin magnitude, considering as input the direction of the accreted gas angular momentum, and the accretion rate. This analysis is therefore simplified with respect to the main text, where spin is tracked on-the-fly, but allows us to highlight the main dependences in a clear way.

In Figure C1 (left) we show the time evolution of the BH spin, angle of the BH spin vector and of the inflow angular momentum with respect to the z-axis, and accretion rate for the first 400 Myr of the galaxy evolution (the “galactic fountain” phase, cf. Fig. 2). As discussed in the main text, high-accretion rates are synchronised with gas cooling and formation of a central rotationally-supported structure, and this is apparent when comparing the two bottom panels. The top two panels show spin magnitude and direction. The black solid curves assume fast alignment, while the red dashed curves show a case with slower alignment ($\nu_2 = \nu_1$). One can notice the different behaviour of the spin direction with time, but the spin magnitude is hardly modified. This is because in the phases of maximum chaos the accretion rate on the BH is low, and therefore the spin magnitude is not affected. In Figure C1 (right) we perform an additional test, where we artificially set the accretion rate to 10 per cent of the Eddington rate at all times, while keeping the information on the direction of the inflow (the third panel from top is the same in both plots). In this experiment, we can assess the effect of prolonged phases of chaotic accretion at high rates (which do not occur in our simulations, due to the synchronisation between cooling, disc formation and BH feeding). Here, in the case of fast alignment (black solid curves) we see that the most chaotic phases of accretion give rise to occasional counter-rotating accretion (e.g., between 250 and 300 Myr) that decrease the spin magnitude. We extend this plot to 600 Myr, where the galaxy reaches a more quiescent regime (“hot bubbles” phase), and a “secular” evolution of the angular momentum direction is reached. By this time, regardless of the assumptions on alignment timescales, the BH spin reaches a steady state at high values.

In conclusion, the alignment timescale is secondary to the dynamics of accretion in determining the BH spin mag-

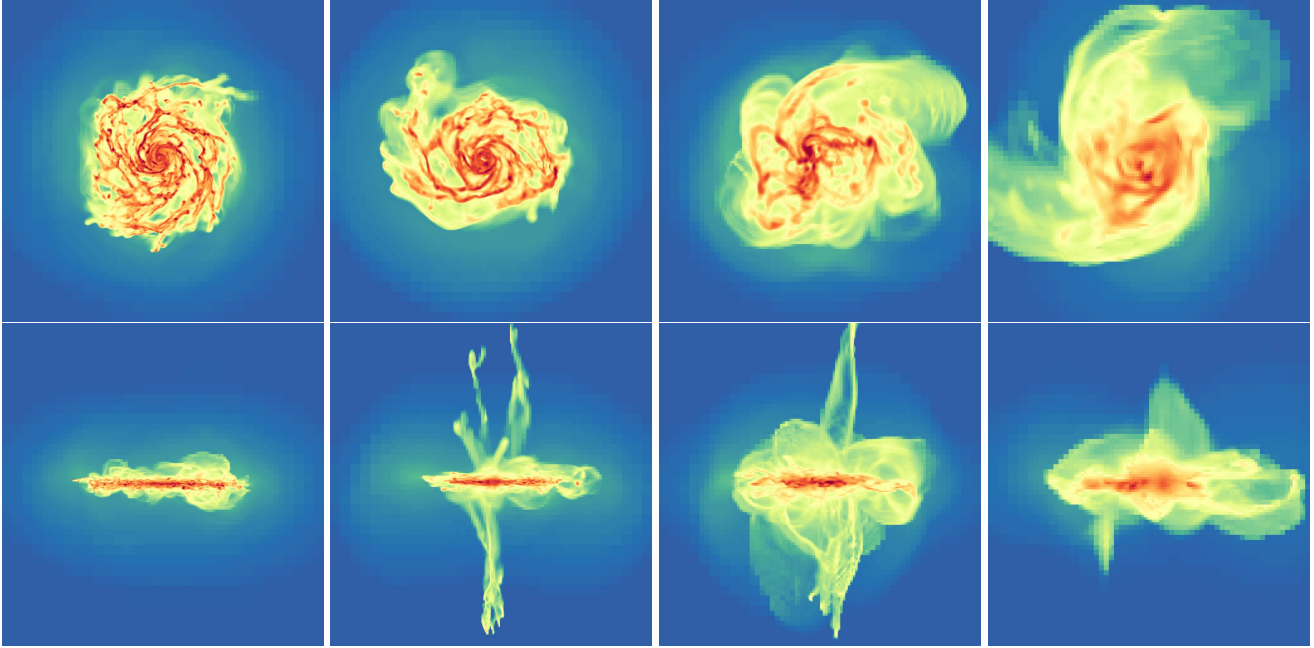


Figure A1. Face-on views (top panels) and edge-on views (bottom panels) of the gas density of the galaxy at $t = 800$ Myr for different resolutions $\Delta x = 10$ pc (left columns), $\Delta x = 20$ pc (middle left columns), $\Delta x = 40$ pc (middle right columns), $\Delta x = 80$ pc (right columns). The same color scaling is applied for all images and images are 10 kpc wide.

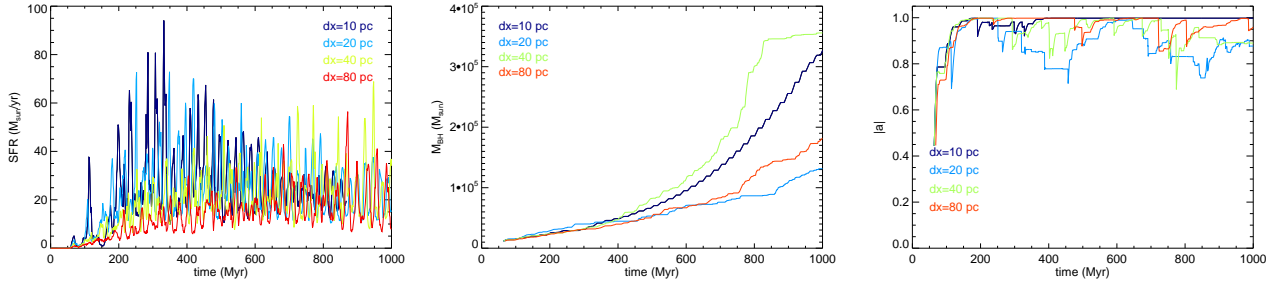


Figure A2. Star formation rate (left panel), BH mass (middle panel) and spin (right panel) as a function of time for different spatial resolutions 10, 20, 40 and 80 pc for the isolated halo initial conditions.

nitude evolution. However, it is the main driver of how fast the spin direction changes, regardless of the accretion rate.

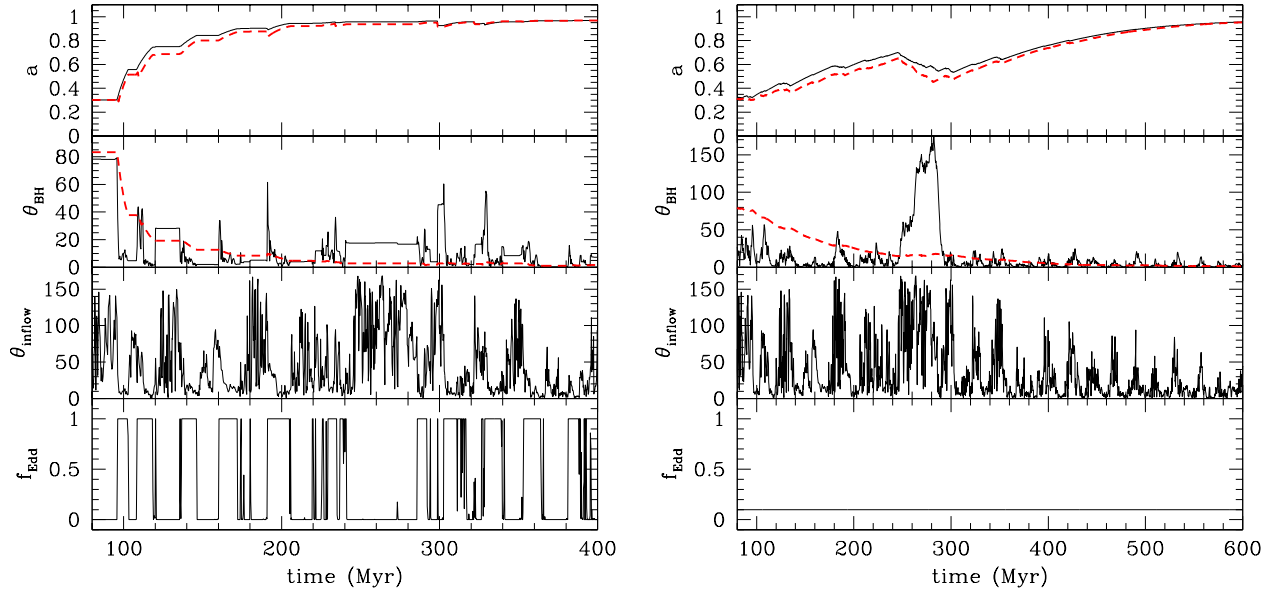


Figure C1. Evolution of BH properties in the isolated galaxy run as a function of time. *Left panel:* we post-process the relative BH alignment and spin magnitude, considering as input the direction of the accreted gas angular momentum and the accretion rate. *Right panel:* the accretion rate is set to 10 per cent of the Eddington rate. The black solid curves track spin magnitude and direction assuming fast spin alignment; the red dashed curves assume instead slow spin alignment.